VU Research Portal

Reduced Phase Models of Oscillatory Neural Networks

Pietras, B.; Daffertshofer, A.

Link to publication in VU Research Portal

Chapter 3
Reduced Phase Models of Oscillatory Neural Networks

Bastian Pietras and Andreas Daffertshofer

Abstract Phase reduction facilitates the analysis of networks of (weakly) coupled oscillators. Synchronization regions can be uncovered and also non-trivial network behavior can be foreseen via the reduced phase dynamics. Phase models have become an essential tool for describing and analyzing rhythmic neural activity. It is widely accepted that in oscillatory neural networks, phase synchronization is crucial for information processing and information routing. Accurately deriving the phase dynamics of interacting neural oscillators is far from trivial. We demonstrate how different reduction techniques of a network of interacting Wilson-Cowan neural masses can lead to different dynamics of the reduced networks of phase oscillators. We pinpoint caveats and sensitive issues in the derivation of the phase dynamics and show that an accurately derived phase model properly captures the collective dynamics. We finally investigate the influence of strong interactions and biologically plausible connectivity structures on the network behavior.

3.1 Introduction

Oscillatory behavior abounds across many different scales of the human brain [17, 18, 80]. To trace and describe these neural oscillations, the development and design of recording techniques and models have benefitted from mutual interaction between experimental and theoretical neuroscientists. Still, linking recordings of brain activity to the underlying neuronal mechanisms remains an urgent challenge. A promising approach to model large-scale brain dynamics builds on networks of

B. Pietras (✉)
Institute of Mathematics, Technische Universität Berlin & Bernstein Center
for Computational Neuroscience, Berlin, Germany
e-mail: pietras@tu-berlin.de

A. Daffertshofer
Faculty of Behavioural and Movement Sciences, Amsterdam Movement
Sciences & Institute for Brain and Behaviour Amsterdam, Vrije Universiteit Amsterdam,
Amsterdam, The Netherlands
e-mail: a.daffertshofer@vu.nl

interacting neural oscillators. By focusing on the corresponding phase dynamics, it is possible to analyze synchronization properties of the network.

As revealed by a plethora of experimental studies relying on both invasive and non-invasive neuroimaging techniques, information processing in the brain is intrinsically linked to synchronization phenomena of oscillatory dynamics [37, 55]. Non-invasive EEG and MEG studies typically depict distributed cortical activity as of large-scale brain networks. Although M/EEG recordings have high temporal resolution, they reflect activity on rather coarse spatial scales given that signals to be perceivable require synchronous neuronal currents of a large number of neurons, commonly of the order of 10^4 to 10^5 cells. The resulting time series of the recordings are duly and extensively analyzed for their extracted phase and amplitude dynamics. Emerging synchronization patterns in the data are then assigned to particular brain functions corresponding to the underlying hypothesis or the behavioral observations. Research on the phase dynamics of cortical oscillatory activity is rather recent compared to amplitude modulations in the M/EEG. However, there are several reports indicating that the phase dynamics play a crucial role for information processing and inter-cortical communication [22, 64, 74, 75, 82, 84].

Phase synchronization also plays an integral part in defining functional connectivity structures of the brain. The technological advance of modern brain imaging methods has led to elucidate the interplay of structural and functional brain connectivity. The structure of anatomical connections between brain areas is widely believed to facilitate temporal synchronization of neural activity, and can lead to spatial patterns of functional connectivity [9, 15, 24, 48]. Yet, the extent to which structure shapes function is still unclear [36, 44]. To unveil functional brain connectivity and communication pathways [10, 33, 54], it is crucial to identify functional modules consisting of remote but synchronized neuronal populations. This can be achieved by analyzing the phase dynamics of the different brain areas.

While extensive data analysis may establish important synchronization properties across the human brain, a comprehensive understanding of the underlying neural mechanisms also requires theoretical models that can be validated and tested against experimental data. Often, heuristic phase models are used as guidelines for inferring neural network dynamics from data. But without a proper derivation of these heuristic models, the results may become questionable. Phase reduction [32, 35, 45, 46, 51, 60, 67, 77] provides a powerful tool to derive phase models from biophysiologically realistic models and to link parameters from the more complex with those from the simpler model in order to identify the key factors for a particular behavioral paradigm. Unfortunately, there is not "the" phase reduction, but one has to choose from a variety of techniques – a recent review can be found in [67]. Even worse, different phase reductions can lead to qualitatively different phase models, that is, reduced phase models may predict different network behavior. For an accurate derivation of a phase model, reduction techniques have to be tailored to the targeted macroscopic observable and the parameter regime under study. Only then one can exploit the full strengths of the reduced phase model. Finally, a word of caution is in order. Phase reduction is strictly valid only for a number of necessary assumptions. Therefore,

one always ought to keep in mind the limitations and range of applicability of an accurately reduced phase model.

In the following, we will demonstrate these aspects in more detail. We will guide our presentation along the example of a network of interacting Wilson-Cowan neural masses, which will be introduced in Sect. 3.2. We will present different phase reduction techniques for a network of weakly coupled oscillators in Sect. 3.3 and show that they may indeed result in different predictions about the collective dynamics. We reported these results previously in an extensive review on network dynamics and phase reduction techniques [67]. Here we add to this by highlighting possible limitations of phase reduction for oscillatory networks in Sects. 3.4 and 3.5. Particular focus lies on network topologies, especially when considering a realistic brain network connectivity structure, and on coupling strengths beyond the weakly perturbed paradigm. We demonstrate why in these cases a reduced phase model may (not) provide valuable information about the actual network dynamics.

## 3.2 Networks of Wilson-Cowan Neural Masses

Considering large-scale oscillatory brain networks, the elementary network components, or nodes, can be assumed to be neural populations consisting of a large number of neurons. From the variety of neural population, or neural mass, models, the seminal Wilson-Cowan neural mass model [88] serves as an exquisite example to derive the phase dynamics in great detail. The Wilson-Cowan model describes the dynamics of the mean firing rates of neuronal populations. At every node $k = 1, \ldots, N$ of the network, we placed properly balanced pairs of excitatory and inhibitory populations with mean firing rates $E_k = E_k(t)$ and $I_k = I_k(t)$, respectively. The nodes are coupled to other nodes through the connections between their excitatory populations [21, 23, 76]. The connection weigths are typically given by a coupling matrix $C = \{C_{jk}\}_{j,k=1,\ldots,N}$. We illustrate the basic structure of this network in Fig. 3.1.

The dynamics at node k takes on the form

$$
\begin{aligned}
\dot{E}_k &= -E_k + \mathcal{S}\left[a_E\left(c_{EE}E_k - c_{EI}I_k - \Theta_E + \frac{\kappa}{N}\sum_{j=1}^{N} C_{kj}g(E_j)\right)\right] \\
\dot{I}_k &= -I_k + \mathcal{S}\left[a_I\left(c_{IE}E_k - c_{II}I_k - \Theta_I\right)\right].
\end{aligned}
\tag{3.1}
$$

The function $\mathcal{S}[x] = (1 + e^{-x})^{-1}$ is a sigmoid function with thresholds Θ_E and Θ_I that need to be exceeded by the total input into neural mass k to elicit firing; the parameters a_E and a_I describe the slopes of the sigmoids. The constants $c_{EE}, c_{EI}, c_{IE}, c_{II}$ quantify the coupling strengths within each (E/I) node and $\kappa \ll 1$ scales the coupling between different nodes. Pairwise interaction between different nodes is mediated through the coupling function $g(E)$, which we choose as $g(E) = E(t) - E^0$. By subtracting an average E^0 (typically, the unstable fixed point

Fig. 3.1 Network of three coupled Wilson-Cowan neural masses. Each node contains excitatory and inhibitory populations, E_k and I_k, that are internally coupled with strengths c_{ij}, $i, j \in \{E, I\}$. Interaction between two neural masses $k \neq j$ occurs via their respective excitatory populations, where C_{kj} denotes the connectivity whether node k receives input from node j
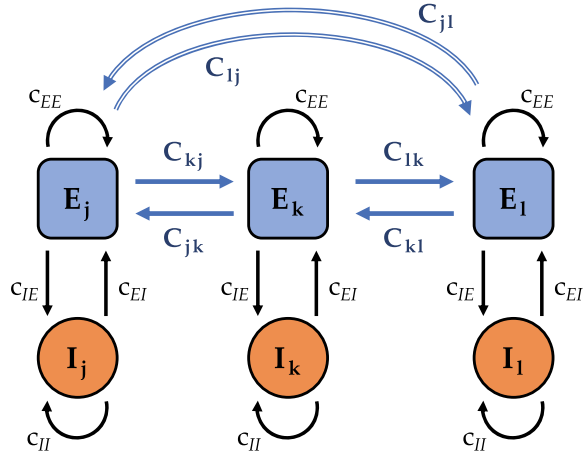
within a stable limit cycle) from the actual firing rate $E = E(t)$, we avoid spurious contributions from other neural masses when they are all synchronized. In general, the interaction within and between different nodes may be time-delayed due to finite signal transmission of, in particular, long-range connections. Allowing for time delays between nodes, or for spatial interaction kernels, yields more intricate coupling dynamics, see, e.g., [47, 73]. For the sake of legibility we here restrict our analysis to instantaneous interactions. We note, however, that phase reduction can also be employed in face of time delays [67, Sect. 10.3.2].

Depending on the choice of parameters, the Wilson-Cowan model Eq. (3.1) can exhibit rich dynamics such as self-sustained oscillations and multi-stability, see, e.g., [14, 45, 67, 88]. Here, we restrict the parameter values (see *Appendix*) to the dynamical regime in which every isolated ($\kappa = 0$) node displays stable limit cycle oscillations. Each point on this stable limit cycle can, in general, be described in terms of a phase and an amplitude. If the attraction towards the limit cycle is sufficiently fast, it is possible to ignore the amplitude dynamics so that the one-dimensional phase variable ϕ_k reliably describes the state of the oscillator not only on the limit cycle, but also in its close vicinity. Moreover, assuming weak coupling between nodes, we can then capitalize on the theory of weakly coupled oscillators [32, 45, 67] to extract the phase dynamics of each node $k = 1, \dots, N$ in form of

$$\dot{\phi}_k = \omega_k + \frac{\kappa}{N} \sum_{j=1}^{N} C_{kj} \Gamma(\phi_k - \phi_j) \tag{3.2}$$

with a natural frequency term ω_k and a phase interaction function $\Gamma(\psi)$ that depends on the phase difference $\phi_k - \phi_j$ between two nodes $k \neq j$. The phase interaction function $\Gamma(\psi)$ is typically periodic in ψ and can thus be expanded in a Fourier series:

$$\Gamma(\psi) = a_0 + a_1 \cos(\psi) + b_1 \sin(\psi) + a_2 \cos(2\psi) + b_2 \sin(2\psi) + \cdots \tag{3.3}$$

The phase dynamics Eqs. (3.2 and 3.3) can subsequently be analyzed with respect to the synchronization behavior of the network. A useful macroscopic observable to describe the network dynamics is the *Kuramoto order parameter* [51]

$$z = R\mathrm{e}^{i\Psi} = \frac{1}{N}\sum_{k=1}^{N}\mathrm{e}^{i\phi_k} , \qquad (3.4)$$

whose absolute value $R = |z|$ takes on values between 0 and 1. $R = 0$ indicates an incoherent state, whereas $R = 1$ indicates a fully synchronized state. Values $0 < R < 1$ indicate partially synchronous collective dynamics. Furthermore, the Fourier coefficients a_n, b_n of the phase interaction function Eq. (3.3) are indicative for particular network behavior. For example, if we consider only the first two harmonics in $\Gamma(\psi)$, i.e. $a_n = b_n = 0$ for $n > 2$, and global coupling, $C_{kj} = 1$ for all $k \neq j$, then it can be shown [20, 49, 67] that the phase model exhibits

- a fully synchronized state for $\kappa b_1 > 0$,
- a balanced two-cluster state for $\kappa b_1 < 0$ and $\kappa b_2 > 0$, and
- slow switching behavior of oscillators between two unbalanced clusters for $\kappa b_1 < 0$, $\kappa b_2 < 0$ and b_1 is comparable in size to b_2.

There may exist additional attractors such as, e.g., three-cluster states or the so-called self-consistent partially synchronous state [20], but general conditions for their existence in terms of the Fourier coefficients $b_{1,2}$ are elusive, so that we rather concentrate on the three regimes above as well as on the incoherent state for $\kappa b_1 < 0$. One can use these insights to predict the collective dynamics of the full network. An accurately reduced phase model is capable of forecasting the transition between synchronous and asynchronous network behavior. Moreover, when focussing on higher harmonics of the phase interaction function $\Gamma(\psi)$, also non-trivial collective dynamics in the original model can be explained with the help of a reduced phase model.

3.3 Phase Reduction of Oscillatory Neural Networks

The ultimate goal of phase reduction is to rigorously establish the mapping between the full dynamics Eq. (3.1) and the reduced phase model Eq. (3.2) by expressing the natural frequency and the phase interaction function in terms of the parameters of the original model Eq. (3.1). Central to phase reductions of weakly coupled neural oscillators is Malkin's theorem [45, 56, 77], which provides a recipe to reduce a dynamical system of the form

$$\dot{\boldsymbol{x}}_k = \boldsymbol{f}(\boldsymbol{x}_k) + \kappa \boldsymbol{g}_k(\boldsymbol{x}_1, \ldots, \boldsymbol{x}_N), \quad \boldsymbol{x}_k \in \mathbb{R}^n, k = 1, \ldots, N, \qquad (3.5)$$

into a phase model Eq. (3.2). As the form of the Wilson-Cowan model Eq. (3.1) does not comply with that of Eq. (3.5), it is compulsory to first transform the original dynamics appropriately. Only then we can employ standard methods [67] to retrieve the phase model Eq. (3.2). We note that the "pre-processing" step can be achieved either numerically or analytically [67, Sects. 4 and 6], giving rise to classifying different phase reduction approaches as either analytic or numerical reduction techniques.

Numerical approaches tend to be more accurate. But their software implementation often computes the necessary properties for phase reduction internally, which leaves the link between the original and the phase model parameters unclear. By contrast, analytic approaches build on subsequent algebraic transformations that yield a rigorous representation of the phase model parameters in terms of the original parameters, although such a representation may become convoluted. The pre-processing of the full dynamics Eq. (3.1) into Eq. (3.5) is based on the idea that close to a particular bifurcation, different models exhibit similar dynamics. Given that the Wilson-Cowan model Eq. (3.1) exhibits oscillatory behavior close to a Hopf bifurcation, we thus aim at transforming Eq. (3.1) into the simplest model that captures the essence of the dynamics close to a Hopf bifurcation point. This simplest model is called Hopf normal form and we can obtain it with a so-called normal form, or center manifold, reduction [45, 59, 67]. There is, however, a caveat. Since we consider not only a single isolated neural oscillator but a network of coupled neural oscillators, we require a *network Hopf normal form*: That is, not only the uncoupled part $f(x)$ in Eq. (3.5) has to be brought into Hopf normal form, but also the coupling function $g_k(x_1, \ldots, x_N)$ has to be identified accordingly subject to all symmetry constraints that are inherent to multiple Hopf bifurcations. Although there is a mathematical proof for such a network Hopf normal form, to the best of our knowledge, no general and exact algorithm for deriving it is at hand. Instead, two approximative schemes have proven fruitful to retain the simplified network Hopf normal form: Kuramoto's reductive perturbation approach and Poincaré's nonlinear transform approach, for details we refer to [67].

Stepping over these often laborious algebraic transforms, there is an alternative analytic approach which becomes exact for weakly coupled oscillators that follow a circular limit cycle: Haken's reduction via averaging [41, 67], see also [13, 40]. For planar oscillatory dynamics close to a Hopf bifurcation, the Jacobian of the uncoupled Wilson-Cowan dynamics Eq. (3.1) evaluated at the unstable fixed point (E_k^0, I_k^0) has a pair of complex conjugate eigenvalues $\lambda_\pm = \mu \pm i\omega$ with positive real part, $\mu > 0$, which corresponds to the distance to the Hopf bifurcation point.[1] We then express the dynamics in terms of the deviations $x_k = \left(E_k - E_k^0(\mu), I_k - I_k^0(\mu)\right)$ around the unstable fixed points. Approximating the sigmoidal activation function $\mathcal{S}$ up to third order and applying some laborious algebraic transforms [67], one can derive a fairly generic form of the dynamics Eq. (3.1) that reads

---

[1] Typically, one measures this distance in parameter space, e.g., in parameter Θ_E such that $\mu = \Theta_E - \Theta_E^H$, where the Hopf bifurcation occurs at $\Theta_E = \Theta_E^H$.

$$\dot{\boldsymbol{x}}_k = \boldsymbol{L}\boldsymbol{x}_k + \boldsymbol{T}^{-1}\boldsymbol{f}\left(\boldsymbol{T}\boldsymbol{x}_k; \mu\right) + \kappa \boldsymbol{T}^{-1} \sum_{j=1}^{N} \boldsymbol{g}\left(\boldsymbol{T}\boldsymbol{x}_k, \boldsymbol{T}\boldsymbol{x}_j\right). \tag{3.6}$$

Here, $\boldsymbol{L}$ is the Jordan real form of the dynamics' Jacobian $\boldsymbol{J}$, $\boldsymbol{T}$ the matrix containing the eigenvectors of $\boldsymbol{J}$. The function $\boldsymbol{f}$ includes all components within node k that contribute to its dynamical change and $\boldsymbol{g}$ covers all the between-node interaction, i.e. the last term of the right-hand side of the $\dot{E}_k$ dynamics in Eq. (3.1) now given as coupling between the nodes $\boldsymbol{x}_k$ and $\boldsymbol{x}_j$. The dynamics Eq. (3.6) exhibits qualitatively the same behaviour as Eq. (3.1), but due to the Jordan real form, a circular symmetry of the limit cycle is imposed on the full dynamics.

In the immediate vicinity of the Hopf bifurcation point, one can exploit the separation of time scales of phase and amplitude dynamics and readily transform Eq. (3.6) into $\boldsymbol{x}_k = (x_k, y_k) = (r_k \cos(\phi_k), r_k \sin(\phi_k))$, where r_k and $\phi_k = \Omega t + \theta_k$ are amplitude and phase (deviations) of the oscillations at node k, which are slowly varying with respect to the (mean) frequency Ω [42], here defined over the eigenvalues at the Hopf point, $\Omega = \omega(\mu = 0)$. Near the onset of oscillations through a supercritical Hopf bifurcation, $r_k \ll 1$ is small and, thus, the right-hand side of Eq. (3.6) is at least of order $\mathcal{O}(r_k)$. Given the slower time scales of r_k and $\theta_k = \phi_k - \Omega t$, one can average over one cycle $T = 2\pi/\Omega$. In line with [21], this direct averaging of the dynamics Eq. (3.6) yields the drastically reduced phase model Eq. (3.2 and 3.3)

$$\dot{\phi}_k = \omega_k + \frac{\kappa}{N} \sum_{k=1}^{N} C_{kj} a_1 \sin(\phi_k - \phi_j) \tag{3.7}$$

with natural frequency $\omega_k = a_E a_I c_{IE} c_{EI} S'_E S'_I - \frac{1}{4}(a_E c_{EE} S'_E + a_I c_{II} S'_I)^2$, first Fourier amplitude $a_1 = \frac{1}{2} a_E S'_E \Lambda_k C_{kj} (R_j/R_k)$, and all other amplitudes vanish: $a_0 = a_n = 0$ for $n > 1$ as well as $b_n = 0$ for all $n \geq 1$. We abbreviated $\Lambda_k^2 = 1 + \rho_k^2$ with $\rho_k = \frac{1}{\omega_k}(a_E c_{EE} S'_E + a_I c_{II} S'_I)$ and $S'_{E/I}$ denotes the first derivative of the sigmoid $\mathcal{S}$ evaluated at the fixed points E_k^0/I_k^0 of Eq. (3.1).

In summary, we have four different phase reduction techniques:

1. Reductive perturbation approach
2. Nonlinear transform approach
3. Direct averaging
4. Numerical/adjoint.

The first two are the analytic approaches that build on a pre-processing step to bring the dynamics in network Hopf normal form. Then, there is Haken's approach that circumvents a rigorous normal form reduction by applying averaging directly to presumably circular dynamics close to the Hopf bifurcation. And finally, one can employ a numerical approach, which capitalizes on Malkin's theorem and provides numerical values for the reduced phase model by solving an associated adjoint problem [16, 29, 31, 32, 45], which has, e.g., been automatized in the software packages XPPAUT [28] or MatCont [26]. In order to compare the different approaches, we will

apply the four different phase reduction techniques to the network of Wilson-Cowan neural masses Eq. (3.1). In the resulting phase models Eq. (3.2), we will concentrate on the reduced natural frequency term ω_k and the first two Fourier harmonics in the phase interaction function Eq. (3.3). Their amplitudes will serve as a quantitative measure of how accurate the phase models are, whereas their relationships with one another provide a qualitative measure indicating whether the reduced phase models result in the correctly predicted collective dynamics; see the end of Sect. 3.2 for a classification of the network's phase dynamics in terms of the Fourier coefficients.

Phase reduction is highly parameter-sensitive

A first litmus test concerns the accuracy of the different phase reduction techniques close to a bifurcation boundary. Center manifold and normal form theory prescribe the exact form of the phase interaction function $\Gamma(\psi)$, see [16]. For the regime near a supercritical Hopf bifurcation, the topological normal form [53] of the dynamics yields a purely sinusoidal phase interaction function, that is, all Fourier coefficients but b_1 in Eq. (3.3) will vanish. The topological Hopf normal form requires further algebraic transformations than the conventional (Poincaré) Hopf normal form, but its essence remains the same: the first Fourier harmonics dominates and higher harmonics tend to zero. In Table 3.1 we show the results of the different phase reduction techniques when the distance to the Hopf bifurcation is as small as $\mu = 0.0003$; here, we chose Θ_E as the bifurcation parameter so that $\mu := \Theta_E - \Theta_E^H$ with Θ_E^H the parameter value where the supercritical Hopf bifurcation occurs. All four reduction techniques can reliably retrieve the correct shape of the phase interaction function with dominant first harmonics and a positive first odd Fourier coefficient $b_1 > 0$, which indicates a fully synchronized state. Moreover, the natural frequency terms coincide for all reduction techniques. Note that the quantitative differences do not influence the qualitative predictions of the network behavior.

When increasing the distance to the Hopf bifurcation point, however, the phase models start to diverge. In Table 3.2, we show exemplary results of the phase model parameters for $\mu = 0.1663$. Only the numerical/adjoint method captures the change of slope of the phase interaction function (whose derivative at $\psi = 0$ is dominated by b_1) and predicts that the fully synchronized state becomes unstable in this parameter region. The other three reduction techniques still predict the synchronous solution,

Table 3.1 Phase models derived with different reduction techniques infinitesimally close to the Hopf bifurcation ($\mu = 0.0003$). The oscillators' natural frequency is ω, and a_n, b_n are the amplitudes of the Fourier components of the phase interaction function Γ

Approach	ω	a_1	b_1	a_2	b_2
Reductive perturbation	0.701	−0.9505	1.1555	−0.0001	0.0013
Nonlinear transform	0.701	−0.9457	1.1382	−0.0009	0.0013
Direct averaging	0.701	−0.6940	0.2140	–	–
Numerical/adjoint	0.701	−0.0472	0.3843	−0.0001	0.0002

Table 3.2 Phase models derived with different reduction techniques away from the Hopf bifurcation ($\mu = 0.1663$). The oscillators' natural frequency is ω, and a_n, b_n are the amplitudes of the Fourier components of the phase interaction function Γ

Approach	ω	a_1	b_1	a_2	b_2
Reductive perturbation	0.728	–0.9505	1.1555	–0.2470	0.3657
Nonlinear transform	1.023	–0.4905	0.1383	–0.0604	0.0503
Direct averaging	1.330	–0.4733	0.2390	–	–
Numerical/adjoint	0.939	–0.4447	–0.2668	–0.0635	–0.0451

although the reduced phase models differ with respect to the amplitude of the harmonics. Compared to the numerical/adjoint method, Poincaré's reduction via nonlinear transforms yields the same orders of magnitude, whereas Kuramoto's reductive perturbation overestimates the second harmonics and the direct averaging by construction does not contain any higher harmonics at all. Strong first harmonics of the phase interaction function will amplify the coupling and thus result in faster (de-)synchronization, depending on the sign of the sinusoidal component. Second and higher harmonics may play a crucial role for clustering. An over- or underestimation of the amplitudes of higher harmonics may hence lead to erroneous predictions of multiple- or one-cluster states.

Accurate phase models capture the true collective dynamics

The farther one moves away from particular bifurcation boundaries, the more the reduced phase models will diverge. Naturally, one seeks a phase reduction technique that reliably recovers the (collective) behavior of the original (network) dynamics. While the accuracy of analytic phase reduction techniques scales with the distance to the bifurcation point (due to the normal form reduction inherent to these two-step reduction approaches [67]), numerical phase reduction techniques, in general, do not suffer this shortcoming and can retain the accuracy across parameter space. For this reason, we will probe the numerical phase reduction and test whether it captures the collective dynamics of the Wilson-Cowan network, indeed.

Following the literature [43, 45], we choose Θ_E and Θ_I as bifurcation parameters and, first, investigate the transition to synchrony as predicted by the slope $\Gamma'(0)$ of the phase interaction function changing from positive (fully synchronous state) to negative values (synchrony becomes unstable). In line with previous results,[2] our findings confirm the general picture that for large parameter regions the fully synchronous state is stable, see the yellow/red regions in Fig. 3.2. In particular, synchrony is stable close to the Hopf bifurcation boundaries of the isolated Wilson-Cowan dynamics (dashed lines in Fig. 3.2).

Second, we try to elucidate the dynamics in parameter regions where the fully synchronized state is no longer stable, see the blue regions and the inset in Fig. 3.2,

---

[2]Hlinka and Coombes [43] showed that the predictions based on the derivative of the numerically reduced phase interaction function agreed almost perfectly with the synchronization properties of the original network, cf. their Figs. 3.6 and 3.7.
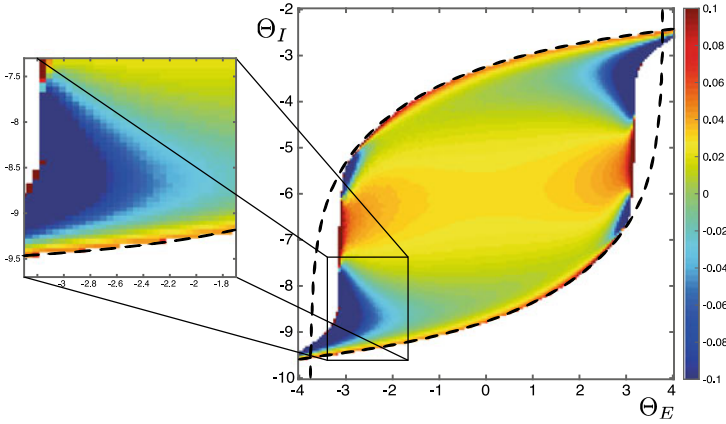
Fig. 3.2 Oscillatory regime of the Wilson-Cowan neural mass model Eq. (3.1) with parameters Eq. (3.8). The colored region of oscillatory behavior lies within the Hopf bifurcation boundaries (black dashed curves) for a single isolated Wilson-Cowan neural mass. The color coding indicates the derivative of the phase interaction function Γ at $\psi = 0$ determining the stability of the fully synchronized state: if $\Gamma'(0) > 0$ the fully synchronized state is stable, and unstable otherwise. We used the numerical/adjoint reduction method to generate this figure

and where previous results did not predict the actual dynamics correctly. Close to the Hopf bifurcation boundary the slope $\Gamma'(0) \approx b_1$ of the phase interaction function is positive and correctly predicts synchronization. Moving upwards in parameter space by increasing Θ_I leads to a change of signs in $\Gamma'(0)$, and we are in the deep blue region in Fig. 3.2, where the fully synchronous state is no longer stable. We fix the parameter $\Theta_E = -3$ and analyze the numerically reduced phase interaction function with respect to higher harmonics for different values of Θ_I. At $\Theta_I = -9.3$, we find that $b_1 > 0$ (stable fully synchronous solution). At $\Theta_I = -8.9$, $b_1 < 0$ and $b_2 < 0$, predicting that the oscillators are evenly spread along the limit cycle, which is also called a stable anti-cluster state. For larger $\Theta_I = -8.7$, the balanced two-cluster state becomes stable ($b_1 < 0$ and $b_2 > 0$); for the exact numerical values see the *Appendix*. To test the predictions of the reduced phase model, we simulated a network of $N = 30$ Wilson–Cowan neural masses with global coupling, $C_{kj} = 1$ for all $k \neq j$, and coupling strength $\kappa = 0.15$. As can be seen in Fig. 3.3, the simulations confirmed the predicted (a) fully synchronized state, (b) an anti-cluster state, i.e. incoherence, and (c) a stable two-cluster state, respectively. The other phase reduction techniques did not only fail to predict the existence of two-cluster states, but they also missed the transition from synchrony to incoherence; cf. Table 3.2.

We can thus conclude that an accurately reduced phase model within its range of applicability can correctly predict collective dynamics of a network of neural oscillators across parameter space. Numerical techniques outperform analytical approaches with respect to accuracy. Still, analytical approaches can yield a direct link between original model parameters and the constituents of the reduced phase model that allow for an immediate prediction of the network state. It is, however, crucial to verify the
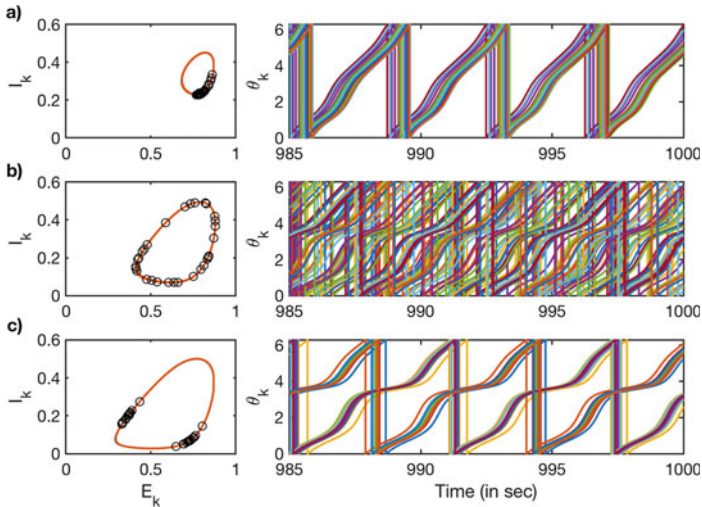
Fig. 3.3 Non-trivial network dynamics of $N = 30$ coupled Wilson-Cowan neural masses. The different network states **a** global synchronization, **b** incoherence, and **c** a balanced two-cluster state were predicted by the reduced phase model using the numerical/adjoint method. Displayed are final ($T_{\text{end}} = 1000$ seconds) conditions ('o') on the uncoupled limit cycle (left column) and the extracted phases (right) for the last 15 seconds. We fixed the coupling strength at $\kappa = 0.15$ and the simulations started from uniformly distributed initial conditions along the uncoupled limit cycle. Parameter values of (Θ_E, Θ_I) are **a** $(-3, -9.3)$, **b** $(-3, -8.9)$ and **c** $(-3, -8.7)$

parameter region where the analytical approaches are applicable. For this reason, we advocate a combination of numerical and analytical phase reduction techniques to provide an accurate picture of the network dynamics and its phase synchronization properties by means of a reduced phase model.

3.4 Phase Reduction in Face of Strong Coupling

The reduction of phase dynamics from a network of coupled oscillators retains its mathematical justification as long as the theory of weakly coupled oscillators applies. However, no rigorous definition of weak coupling exists, nor a concrete limit of the coupling strength at which the character of interaction switches from weak to strong. Usually, phase reduction is achieved with the tacit understanding that each isolated dynamical system already displays stable limit cycle oscillations, which is a necessary condition for the theory of weakly coupled oscillators to hold [5, 45]. However, in some cases it is the coupling between systems that induces oscillations. Smale was among the first to investigate the emergence of oscillations via a Hopf bifurcation due to diffusive coupling [79]. On the other hand, coupling between systems can also make oscillations cease. Ermentrout and Kopell reported this kind

of oscillation death for a chain of Wilson-Cowan neural masses [30], see also the work by Daffertshofer and van Wijk on a (heterogeneous) network of Wilson-Cowan neural masses [23]. Those coupling-induced effects only occur for reasonably large coupling strengths, and a straightforward identification of the phase dynamics as within the theory of weak coupling is not possible. While sufficiently weak coupling ensures that the shape and the frequency of the limit-cycle orbits remain almost unchanged, strong coupling leads to non-negligible amplitude effects. These can destabilize synchronized states, quench oscillations, or cause collective chaos, and a phase reduction has only been proposed for quite restrictive assumptions; see [52] and the references therein. Hence, phase-amplitude reductions [19, 78, 87], see also [57, 67] for reviews, have to be employed that also take interactions between phase and amplitude dynamics into account. The theory of weakly coupled oscillators additionally requires that the actual trajectories of the oscillators are always close to the isolated limit-cycle solution. While reduction methods exist that allow for a phase reduction farther away from the underlying periodic orbit, see, e.g., [57, 67, 89], we here try to answer the question whether appropriate conventional phase models can still capture coupling-induced collective dynamics.

Oscillation birth and clustering

To investigate coupling-induced behavior, it appears illustrative to start with two coupled identical Wilson-Cowan neural masses. In Fig. 3.4 we show the bifurcation diagram with respect to the coupling strength. Without coupling, $\kappa = 0$, the dynamics Eq. (3.1) feature only one stable stationary solution (black solid line). Increasing the coupling strength induces oscillations through a (double) Hopf bifurcation (red dot). The critical coupling strength κ_H can also be determined analytically, see the *Appendix* but also [4]. In our example, it is considerably small with $\kappa_H = 0.00531$ (note that we did not rescale the coupling by a factor $1/N$). In this coupling-induced oscillatory regime, the initial conditions can have a major impact on the resulting dynamics. For small coupling strengths $\kappa < 0.6$ (see green dot), the two Wilson-Cowan neural masses evolve from any initial conditions either into the same limit cycles or into the low activity resting state (blue solid curve). For larger coupling strengths, however, only identical initial conditions result into the same (red) limit cycles. Different initial conditions for the two coupled neural masses may still lead to stable oscillations, but the respective limit cycles of each neural mass can differ in amplitude and shape (cf. the green curves in Fig. 3.4). Moreover, these distinct oscillations that resulted from distinct initial conditions are stable beyond a critical coupling strength at which those oscillations from identical initial conditions have ceased to exist (through a fold bifurcation of limit cycles, see the inset in Fig. 3.4). From the point of view of oscillation quenching mechanisms [50], the onset of (identical) limit-cycle oscillations of the two Wilson-Cowan neural masses for small coupling strengths is a mechanism inverse to amplitude death. Larger coupling induces a symmetry breaking from two identical to two distinct limit cycles, and thus drives the system into an oscillation death-related regime. Note, however, that the Wilson-Cowan neural masses keep oscillating around the same, spatially uniform center,
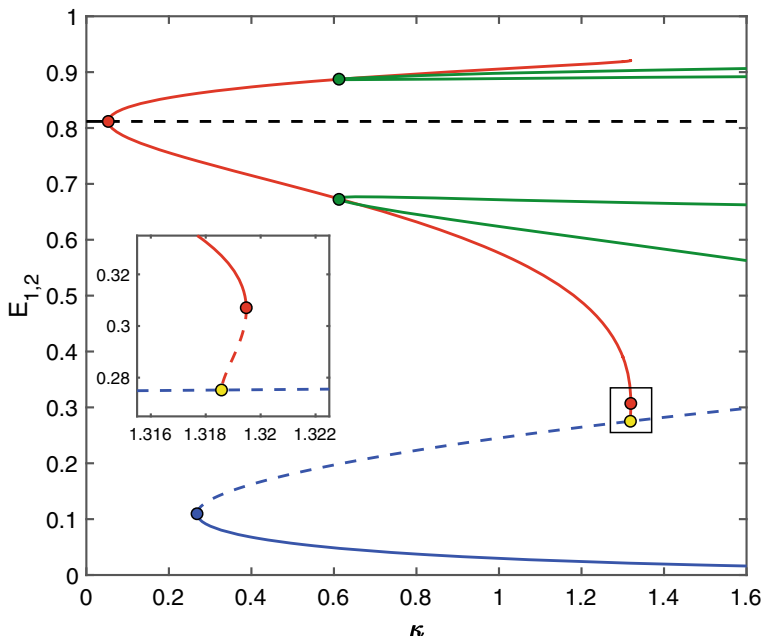
Fig. 3.4 Bifurcation diagram of two coupled identical Wilson-Cowan neural masses with parameters $(\Theta_E, \Theta_I) = (-3, -9.4)$. At low coupling, the units are at rest (black solid curve). Oscillations emerge at a double Hopf bifurcation (red dot), where the resting state becomes unstable (black dashed). The red curves display upper and lower limit of the limit cycles. Beyond the green dot, identical initial conditions of the two units evolve towards identical limit cycles (red curve) that are destroyed through a fold bifurcation of limit cycles (second red dot), whereas non-identical initial conditions lead to two distinct oscillatory solutions (with upper/lower limits on either the outer or inner branches of the green curves) that remain stable for large coupling strengths, for which identical initial conditions lead into a low-activity resting state (blue solid).The yellow dot represents a homoclinic bifurcation, induced through the unstable saddle (blue dashed) that emerged through a saddle-node bifurcation of fixed points (blue dot)

and that beyond a critical coupling strength, oscillations cease and give rise to a homogeneous steady state, which is coined amplitude death in the literature [50].

Based on the brief analytic insights concerning two coupled oscillators, we anticipate that coupling-induced effects will increase the intricacy of larger networks of strongly coupled oscillators. To illustrate this, we simulated a fully connected network of 30 identical Wilson-Cowan neural masses with random initial conditions. Figure 3.5 displays the network behavior for different coupling strengths. Without coupling, the dynamics evolve from random initial conditions towards the stationary solution given by the fixed point in Fig. 3.5 (top left panel). The dynamics of the (absolute value of the) Kuramoto order parameter R reflects the transient oscillatory dynamics from the initial conditions into the fixed point solution, where the phases of
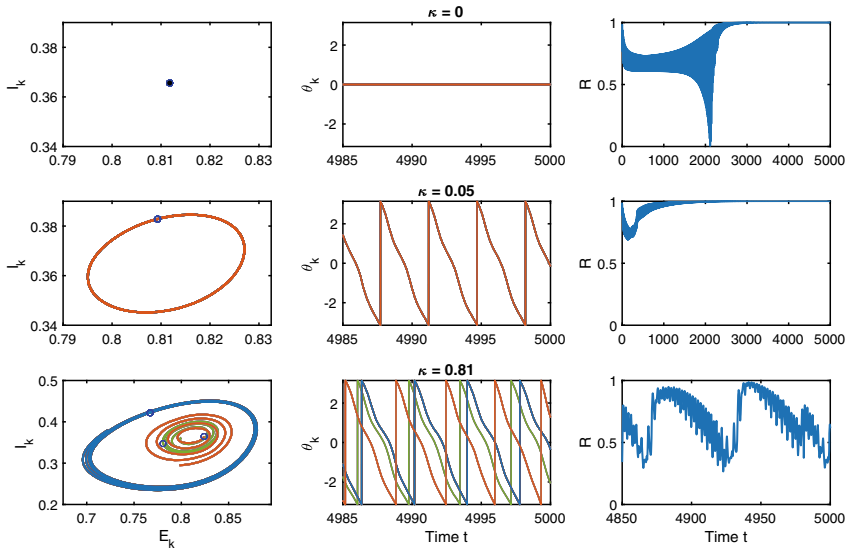
Fig. 3.5 Coupling-induced behavior of $N = 30$ globally coupled identical Wilson-Cowan neural masses with parameters $(\Theta_E, \Theta_I) = (-3, -9.4)$. Without coupling (top row), only the resting state is stable. At low coupling strength $\kappa = 0.05$ (middle row), all neural masses synchronize on the same limit cycle. At high coupling strength $\kappa = 0.81$ (bottom row), the neural masses form three clusters on distinct limit cycles and show intermittent synchronization. Left: dynamics of all neural masses in the $E_k - I_k$ plane for the last $t = 15$ seconds. Middle: extracted phases of all neural masses. Right: absolute value of the Kuramoto order parameter displaying phase synchronization of the network. See the *Appendix* for details about the network simulation and analysis.

the oscillators stay constant (after $t \approx 2500s$). For $\kappa = 0.05$, the coupling is already strong enough to lead to maintained oscillatory dynamics. The Wilson-Cowan neural masses become fully synchronized and oscillate on identical limit cycles (middle row in Fig. 3.5). For even stronger coupling, the coupling-induced oscillations become more complex. Clusters of oscillators emerge, which evolve on distinct oscillatory trajectories. In Fig. 3.5 (bottom row), the oscillatory neural masses have formed three groups that consist of different numbers of oscillators. Within each group, all oscillators are perfectly synchronized and follow the same (quasiperiodic) dynamics (see the middle and left panel, respectively). These dynamics differ, however, across groups. Note that although the Kuramoto order parameter exhibits complex oscillatory dynamics around a value that may indicate some partially synchronous state, it is impossible to infer from it the correct network behavior of three oscillating clusters.

Quenching of oscillations and quasiperiodic dynamics

To investigate the quenching of oscillations, we chose parameters such that (a) a single isolated Wilson-Cowan neural mass exhibits stable limit-cycle oscillations and
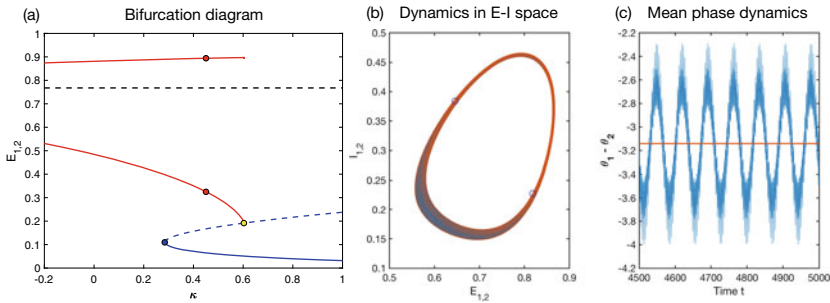
Fig. 3.6 Amplitude death and quasiperiodic behavior of two coupled identical Wilson-Cowan neural masses. **a** Bifurcation diagram similar to Fig. 3.4, but starting with stable limit cycle oscillations without coupling. Oscillation death occurs via a homoclinic bifurcation (yellow dot) for identical initial conditions. The red dots denote the emergence of quasiperiodic behavior for distinct initial conditions. In **b** quasiperiodic behavior of the two Wilson-Cowan neural masses (final condition of the two limit cycles shown as 'o') is depicted for coupling strength $\kappa = 0.475$. **c** The phase difference $\psi(t) = \theta_1(t) - \theta_2(t)$ (blue line) fluctuates around the mean $\bar{\psi}(t) = -\pi$ (orange), which indicates an incoherent state.

(b) weak global coupling leads to an incoherent, that is, asynchronous solution. The bifurcation diagram for two coupled identical oscillators with respect to the coupling strength is shown in Fig. 3.6. For identical initial conditions, the red curves represent the upper and lower limit of the amplitude of identical limit cycles, on which the two oscillators are phase-locked with a constant phase difference of $|\theta_1(t) - \theta_2(t)| = \pi$, as expected for weak coupling. The oscillations cease via a homoclinic bifurcation (yellow dot), in contrast to the fold bifurcation of limit cycles in the previous example. For distinct initial conditions, we find again two different oscillatory regimes: at low coupling strengths, the anti-phase periodic solutions evolve on the same limit cycle. However, for coupling strengths larger than $\kappa \approx 0.45$ (red dot) each neural mass exhibits quasiperiodic behavior (Fig. 3.6b). Remarkably, the mean phase difference $\bar{\psi}(t) = \lim_{T\to\infty} \int_0^T |\theta_1(t) - \theta_2(t)|dt = \pi$ stays constant, see orange line in Fig. 3.6c, which underlines that the oscillators remain incoherent.

As before, we simulated the network dynamics and confirmed the analytic predictions extrapolated from two coupled Wilson-Cowan neural masses to a larger network. Results are shown in Fig. 3.7. The parameters Θ_E, Θ_I are chosen such that the reduced phase model predicts asynchronous network dynamics for low coupling strengths, as is demonstrated by the simulations (top row). Increasing the coupling strength leads, first, to a general increase in network synchronization as indicated by the Kuramoto order parameter and, then, to quasiperiodic dynamics (middle row). The oscillators follow the same quasiperiodic trajectories spanning an annulus-shaped region in state space (similar to the behavior as shown in Fig. 3.6b). Note that although the phases of the oscillators tend to get closer to each other, the coupling is not strong enough to completely synchronize them also with respect to their amplitudes. Increasing the coupling strength even more, eventually results in destroying the network oscillations: the oscillatory dynamics of the individual
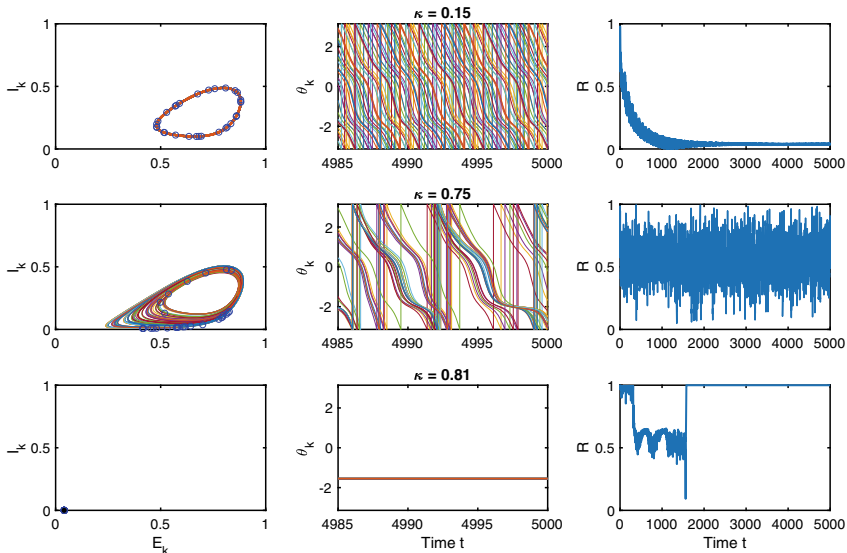
Fig. 3.7 Coupling-induced behavior of $N = 30$ globally coupled identical Wilson-Cowan neural masses with parameters $(\Theta_E, \Theta_I) = (-3, -9)$. At low coupling strength $\kappa = 0.15$ (top row), all neural masses desynchronize on the same limit cycle as predicted by the phase model. At intermediate coupling strength $\kappa = 0.75$ (middle row), oscillators move along quasiperiodic trajectories and tend to synchronize. At very high coupling strength $\kappa = 0.81$ (bottom row), oscillation death occurs and the neural masses run into a low activity resting state. Left: dynamics of all neural masses in the $E_k - I_k$ plane for the last $t = 15$ seconds. Middle: extracted phases of all neural masses. Right: absolute value of the Kuramoto order parameter displaying phase synchronization of the network. See the *Appendix* for details about the network simulation and analysis.

Wilson-Cowan neural masses collapse into the same low activity state (bottom row in Fig. 3.7). As before, the oscillation quenching mechanism is amplitude death [50]. Time-delayed interactions can also induce amplitude death, typically by stabilizing a specific homogeneous state [50]. Incorporating time delays in our setup will affect the bifurcation structure and may lead to interesting new phenomena, especially for large coupling strengths. For weak coupling, we hypothesize that the predictions on network synchronization based on a properly reduced phase model remain valid—given that time delays are taken into account during the phase reduction as, e.g., in [67, Sect. 10.3.2].

3.5 Phase Reduction in Face of Complex Structural Connectivity

Up to now, we have only considered globally coupled Wilson-Cowan neural masses with a trivial connectivity matrix, $C_{kj} = 1$ for all $k \neq j$. A realistic connectivity

structure in neural networks can have significant consequences for the collective dynamics, see, e.g., [1–3, 7, 11, 12, 27, 38, 61, 62, 68, 71, 72, 81]. A network topology, i.e. how the nodes of the network are connected, that deviates from global, all-to-all coupling, may render many results about predicted network behavior no longer valid. In some cases, the reduced phase interaction function Γ in combination with the connectivity matrix can still provide important information about the collective dynamics of a realistically connected network, e.g., about (remote) synchronization, see [25, 34, 58, 63, 69]. The Kuramoto model of phase oscillators where $\Gamma(\psi) = \sin(\psi)$ has been extensively studied on complex networks, see, e.g., the review by Rodrigues et al. [70]. More recently, it could also be shown how time delays shape the phase relationships in oscillatory networks with realistic connectivity structure [65, 66]. Some questions, however, still remain unanswered, e.g., how structure shapes function, what the constituents for synchrony are, or what drives a network into a chaotic state.

To illustrate how realistic structural connectivity—as derived, e.g., from diffusion tensor imaging (DTI)—adds to the complexity of the dynamics of neural networks, we compared the dynamics of the full Wilson-Cowan model Eq. (3.1) with the reduced phase model Eq. (3.2) for three different coupling topologies: a fully connected homogeneous network, an anatomical network reported by Hagmann and co-workers [39], and a network with small-world topology generated by the Watts-Strogatz model [86]. For the fully connected homogeneous network (i.e. global connectivity), we considered the adjacency values $C_{kj} = 1$ for all $k \neq j$, but set $C_{kk} = 0$ to exclude self-connections. For the Hagmann network, we used a DTI dataset to build a realistic network topology of the human cerebral cortex as described by Hagmann et al. [39]. To extract the "structural core" of anatomical connections, the original 998 cortical regions were assigned to a 66-node parcellation scheme and averaged over five subjects. The binary coupling matrix $C = \{C_{kj}\}$ was obtained by subsequently thresholding the weighted and undirected network gained through parcellation and
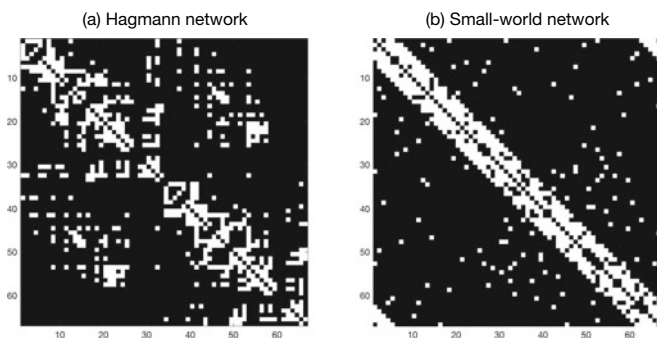

Fig. 3.8 Coupling matrices $C = \{C_{kj}\}$ for **a** the Hagmann dataset and **b** the small-world topology with $N = 66$ nodes. We generated the small-world network by using the same graph-theoretical properties as of the Hagmann network (average degree = 10, rewiring probability = 0.2). White pixels denote a link between nodes k and j, $C_{kj} = 1$
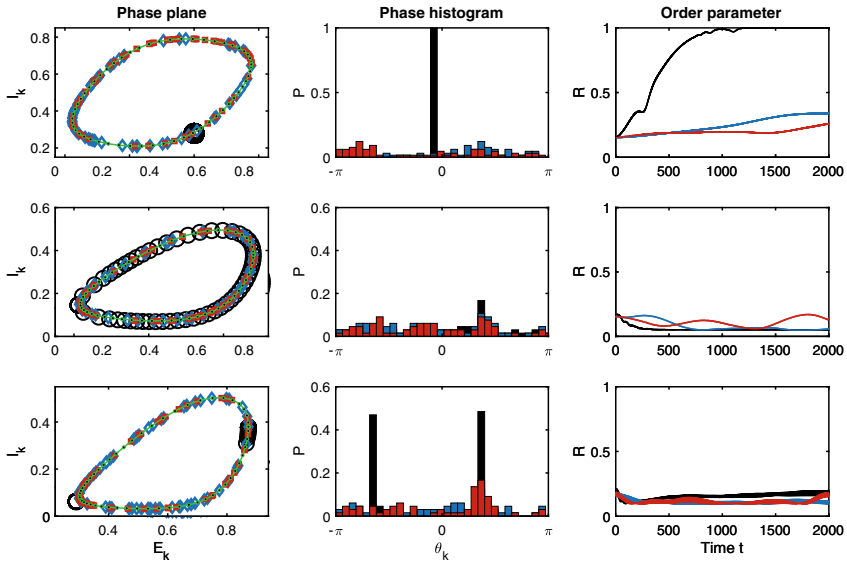
Fig. 3.9 Simulation of the Wilson-Cowan dynamics at coupling strength $\kappa = 0.15$ for regimes as predicted by the numerically reduced phase model: synchronization (top row), asynchrony (middle) and two-cluster state (bottom); see Tables 3.3, 3.4 and 3.5 in the *Appendix*. Left: final ($T = 2000$) position of all $N = 66$ Wilson-Cowan oscillators on the unperturbed limit cycle (green) with random initial conditions (black dots). Middle: histogram of the phases extracted from the final positions of the oscillators. Right: phase synchronization of the network measured in terms of the absolute value of the Kuramoto order parameter with a moving average of 20 seconds. Colors indicate full connectivity (black, circles), small world (blue, diamonds), and Hagmann (red, squares)

averaging, see Fig. 3.8 (panel a) [23, 83]. Analyzing the coupling matrix C further showed that the Hagmann network featured characteristics of a small-world network with average node-degree 10. For comparison, we thus generated a small-world network artificially by employing the procedure as introduced by Watts and Strogatz [86]: starting from an ordered network on a ring lattice with nodes connected to only a few direct neighbors, we subsequently rewired connections to random nodes with a certain probability (in our case 0.2) until we obtained a small-world network with the same average node-degree, see Fig. 3.8 (panel b). In other words, by adding a few random nodes in an ordered network, we thus created a small-world network featuring high clustering and low path length, which yields particular dynamical and synchronization properties that are appealing for their use in neuroscience [3, 6, 8, 85].

We then simulated the Wilson-Cowan networks with the three different coupling matrices. We chose parameter sets for which the reduced phase model (with global coupling) predicted synchronization, incoherence and cluster states. In Fig. 3.9 we show the network simulations for each of the three parameter regimes (top row: synchronization, middle: incoherence, bottom: balanced two-cluster state) and for each of the three coupling matrices (black: homogeneous coupling, blue: small-word, red:
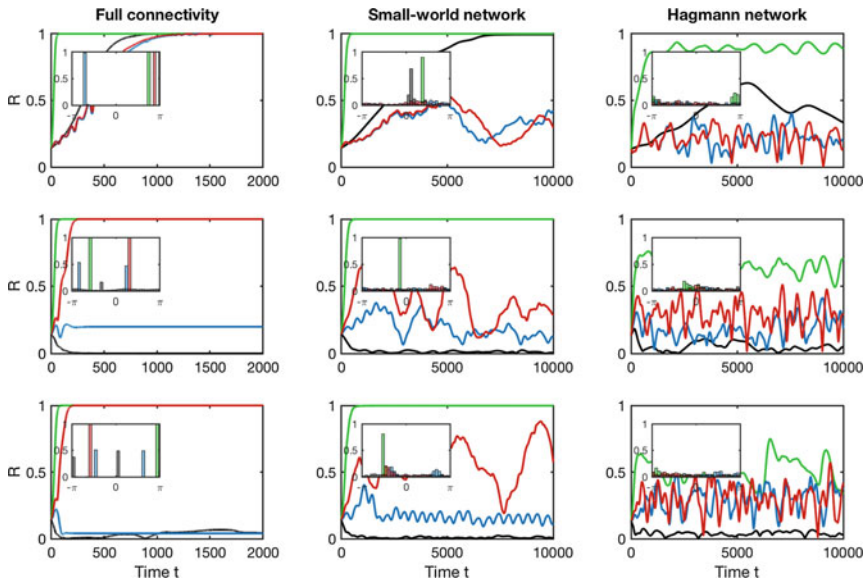
Fig. 3.10 Simulation of the reduced phase models as given in Tables 3.3, 3.4 and 3.5 at coupling strength $\kappa = 0.25$ with full (left column), small-world (middle) and Hagmann network connectivity (right) for parameter regimes where the numerically reduced phase model with global coupling predicts synchronization (top row), asynchrony (middle) and two-cluster state (bottom) Insets show histograms at final ($T = 2000$ for full connectivity, and $T = 10000$ otherwise) phase distribution for $N = 200$ oscillators ($N = 66$ for Hagmann network). Colors correspond to numerical reduction approach (black), direct averaging (green), reductive perturbation approach (red), and nonlinear transform approach (blue)

Hagmann). The more complex connectivity structures lead to macroscopic dynamics that become indistinguishable from one another; cf. the red and blue graphs corresponding to small-world and Hagmann networks, respectively. Only in the case of a fully connected homogeneous network (black graphs), the actual dynamics match the predictions of the (numerically) reduced phase model. Furthermore, we simulated the different phase models as derived with each of the four reduction techniques. The numerically reduced phase dynamics (black graphs) correctly captures the original Wilson-Cowan dynamics for full connectivity, see the left column in Fig. 3.10. For non-trivial connectivity structures, however, none of the phase models can follow the predictions based on the phase interaction function Γ. While for the small-world network (middle column) the simulations hint slightly at the synchronous, asynchronous and two-cluster regimes, respectively from top to bottom, the observed dynamics on the Hagmann network appear arbitrary. Note that the direct averaging technique (green graphs) leads to synchronous collective dynamics for almost all parameter settings and connectivity structures. The two analytic techniques diverge for full connectivity: the reductive perturbation approach (red) leads to a fully synchronized state, whereas the nonlinear transform approach (blue) results in a two-cluster state,

cf. the phase histograms of the final conditions (insets in Fig. 3.10). But for the small-world and Hagmann networks, these two techniques converge to the same resulting behavior. For details about the simulations see the *Appendix*.

In a nutshell, we can conclude that topology effects overcome otherwise precise predictions of the phase model such that even the least accurate direct averaging method does not perform worse than the other techniques.

3.6   Conclusion

Phase reduction is a powerful tool to simplify the dynamics of complex networks of neural oscillators. The reduced phase model allows a reliable prediction of various network behavior. Not only the transition between an incoherent state and a fully synchronized state can be revealed, but, by taking higher harmonics of the reduced phase interaction function into account, also non-trivial collective behavior can be forecast such as cluster states or slow-switching between clusters.

There does not, however, exist "the" phase reduction, but one has to choose from a variety of phase reduction techniques. The different reduction methods can broadly be classified as numerical and analytical phase reduction techniques. We compared different phase reduction techniques of oscillatory neural networks and showed that close to a particular bifurcation boundary, all reduction techniques retrieve the same qualitative results. Further away from bifurcation boundaries, different techniques start to diverge and one has to pay careful attention to whether, e.g., an analytically reduced phase model indeed captures the correct network behavior. We advocate a combination of numerical and analytical approaches to ensure the sought-for accuracy of the phase model while, at the same time, allowing for a direct mapping between the parameters of the neural network model with those of the reduced phase model. By this, one can identify key parameters of the neural network that have major influence on the synchronization properties of the network.

Furthermore, we showed that phase reduction has important limitations when facing strong coupling and realistic connectivity structure. Although augmented phase reduction and phase-amplitude reduction techniques for single oscillators have seen strong advances in recent years [57, 67], their extension to oscillatory networks has yet to be achieved. We illustrated some peculiar characteristics of coupling-induced behavior, such as birth and death of oscillations, and highlighted how insights about the dynamics of two strongly-coupled oscillators can be used to explain network effects such as clustering into groups of various sizes and quasiperiodic dynamics on a network level. For small coupling strengths, predictions by the reduced phase model remain valid. For stronger coupling, the validity of the reduced phase model breaks down. A reasonably good proxy for a critical coupling strength beyond which the phase model loses validity, can be obtained from the dynamics of two coupled identical systems. We hypothesize that this critical coupling strength is exceeded once the coupling-induced behavior becomes more complex, that is, when identical initial conditions result in distinct oscillatory dynamics of the two oscillators.

As to connectivity effects, we have to conclude that a reduced phase model cannot account for changes in the underlying network topology. Realistic structural connectivity has devastating impact on the network dynamics in that the collective behavior drastically differs from that for homogeneous connectivity. Even the numerically reduced phase model was no longer capable of capturing the actual network dynamics and could also no longer outperform the other reduction techniques. All phase reduction techniques performed equally well. Neither the Kuramoto order parameter dynamics nor the phase diagrams were informative for the network states with realistic structural connectivity. It may hence be helpful to first identify meaningful observables that link structure and dynamics of the network. Once this has been achieved for networks of general oscillators vis-á-vis networks of phase oscillators, we may be able to answer the question whether a reduced phase model retains the same structural-dynamical properties of the full network and can thus be used to predict also exotic network effects that arise due to complex structural connectivity.

Appendix

Following the literature [43, 45], we considered Θ_E and Θ_I as bifurcation parameters and fixed the other parameters of the Wilson-Cowan neural mass model Eq. (3.1) as

$$a_E = 1, a_I = 1, c_{EE} = c_{EI} = c_{IE} = 10, c_{II} = -2. \tag{3.8}$$

The numerical phase reduction technique correctly predicts the stability of the globally synchronized state for parameters $(\Theta_E, \Theta_I) = (-3, -9.38)$, of the incoherent state for $(\Theta_E, \Theta_I) = (-3, -8.9)$, and of the balanced two-cluster state for $(\Theta_E, \Theta_I) = (-3, -8.7)$. Tables 3.3, 3.4 and 3.5 provide the numerical values of the Fourier coefficients of the numerically reduced phase interaction function $\Gamma(\psi)$, Eq. (3.3), together with those derived along the analytic phase reduction techniques.

Coupling induced behavior
We investigated the birth and death of oscillations due to the strength of coupling between oscillators. The bifurcation diagrams in Figs. 3.4 and 3.6 were created with MatCont [26] for two identical Wilson-Cowan neural masses following the dynamics

Table 3.3 Phase models derived for different approaches at $\Theta_E = -3$, $\Theta_I = -9.38$

Approach	ω	a_1	b_1	a_2	b_2
Reductive perturbation	1.800	–0.3666	0.0251	–0.0006	0.0015
Nonlinear transform	1.800	–0.3675	0.0260	–0.0006	0.0015
Direct averaging	1.800	–0.1280	0.5739	–	–
Numerical/adjoint	1.800	–0.0413	0.0339	–0.0002	–0.0001

Eq. (3.1). The coupling-induced Hopf bifurcation can be determined analytically by inspecting the eigenvalues of the Jacobian of the (high-activity) resting state (E^0, I^0). The Jacobian has the form

$$J = \begin{pmatrix} -1 + c_{EE}S_{E1} & -c_{EI}S_{E1} & \kappa S_{E1} & 0 \\ c_{IE}S_{I1} & -1 - c_{II}S_{I1} & 0 & 0 \\ \kappa S_{E1} & 0 & -1 + c_{EE}S_{E1} & -c_{EI}S_{x1} \\ 0 & 0 & c_{IE}S_{I1} & -1 - c_{II}S_{I1} \end{pmatrix}$$

where we introduced the abbreviations $S_{E1} = a_E S' \left[a_E \left(c_{EE} E^0 - c_{EI} I^0 - \Theta_x \right) \right]$ and $S_{I1} = a_I S' \left[a_I \left(c_{IE} E^0 - c_{II} I^0 - \Theta_y \right) \right]$ and (E^0, I^0) denotes the fixed point solution. The eigenvalues $\lambda_{1,2,3,4}$ of J can readily be found and the Hopf bifurcation point at $\mathrm{Re}(\lambda_{1,2}) = 0$, $\mathrm{Re}(\lambda_{3,4}) < 0$ identified. The critical coupling strength is $\kappa_H \approx 0.053$, in perfect agreement with our computations using MatCont [26].

Network simulations
The network simulations for Fig. 3.3 of $N = 30$ globally coupled, identical Wilson-Cowan neural masses have been initialized by choosing initial conditions on the uncoupled limit cycle such that the phase synchronization (real-valued Kuramoto order-parameter) was $R = 0.15$. The dynamics Eq. (3.1) have then been run with parameter values given by Eq. (3.8) and coupling strength $\kappa = 0.15$ using an Euler-Mayurama scheme over $T = 1000s$ ($T = 5000s$ for panels b and c) with stepsize $dt = 0.001s$ and noise strength $\sigma = 10^{-8}$.

For the network simulations in Figs. 3.5 and 3.7, we used again $N = 30$ globally coupled identical Wilson-Cowan neural masses and set the coupling strength as indicated in the captions. We chose random initial conditions in the basin of attrac-

Table 3.4 Phase models derived for different approaches at $\Theta_E = -3$, $\Theta_I = -8.9$

Approach	ω	a_1	b_1	a_2	b_2
Reductive perturbation	1.276	–0.3666	0.0251	–0.0381	0.0868
Nonlinear transform	1.263	–0.4592	0.0908	–0.0194	0.0562
Direct averaging	1.276	–0.2283	0.4600	–	–
Numerical/adjoint	1.267	–0.4436	–0.1244	–0.0077	-0.0184

Table 3.5 Phase models derived for different approaches at $\Theta_E = -3$, $\Theta_I = -8.7$

Approach	ω	a_1	b_1	a_2	b_2
Reductive perturbation	1.078	–0.3666	0.0251	–0.0522	0.1187
Nonlinear transform	1.079	–0.4945	0.1217	–0.0191	0.0574
Direct averaging	1.078	–0.2649	0.4245	–	–
Numerical/adjoint	1.062	–0.5877	–0.2324	–0.0304	0.0135

tion of the attracting high-activity resting state, and of the attracting limit-cycles, respectively, and found the same behavior for a range of different random selections of initial conditions. We simulated Eq. (3.1) over $T = 1000s$ with a time-step $dt = 0.0005s$ using an Euler-forward scheme. Simulations using a Runge-Kutta fourth order scheme resulted in the same dynamics. We extracted the phases from each Wilson-Cowan node (E_k, I_k) using the function $\theta_k = atan2(x_k, y_k)$, where $x_k = E_k - E^0$ and $y_k = I_k - I^0$ denote the deviations from the unstable fixed point. The degree of synchronization is measured as phase coherence in terms of the real-valued Kuramoto order parameter, $|z(t)| = |\sum_k \exp(i\theta_k(t))|$. Both the phase values as well as the Kuramoto order parameter have been extracted on a coarser time scale with $dt = 0.1s$.

For the network simulations in Fig. 3.9, we simulated the dynamics Eq. (3.1) for $N = 66$ identical Wilson-Cowan neural masses with coupling strength $\kappa = 0.15$ over $T = 2000s$ with a time step of $dt = 0.0005s$ using an Euler-forward scheme, and extracted the phases and the Kuramoto order parameter as described above. We used a moving average of $20s$ to better compare the evolution of the degree of synchronization for the different networks. We also simulated the corresponding phase dynamics Eq. (3.2) of the reduced phase models on the different network structures and in the three dynamical regimes. The Fourier coefficients for the respective phase models are listed in Tables 3.3, 3.4 and 3.5. Since amplitude effects cannot occur in the phase model, we set the coupling strength to $\kappa = 0.25$, to accelerate possible synchronization transitions and to better identify transient dynamics. Moreover, we increased the network size for full and small-world network connectivity to $N = 200$ to reduce finite-size effects. The phase dynamics were simulated for $T = 10000s$ with a time step $dt = 0.001s$ using an Euler-forward scheme. We computed the Kuramoto order parameter for each time step $dt = 0.1s$ and showed the final phase distribution in a histogram plot with 31 bins.

References

1. G. Ansmann, R. Karnatak, K. Lehnertz, U. Feudel, Extreme events in excitable systems and mechanisms of their generation. Phys. Rev. E **88**, 052911 (2013)
2. G. Ansmann, K. Lehnertz, U. Feudel, Self-induced switchings between multiple space-time patterns on complex networks of excitable units. Phys. Rev. X **6**, 011030 (2016)
3. A. Arenas, A. Díaz-Guilera, J. Kurths, Y. Moreno, C. Zhou, Synchronization in complex networks. Phys. Rep. **469**(3), 93 (2008)
4. D.G. Aronson, G.B. Ermentrout, N. Kopell, Amplitude response of coupled oscillators. Phys. D **41**(3), 403 (1990)
5. P. Ashwin, S. Coombes, R. Nicks, Mathematical frameworks for oscillatory network dynamics in neuroscience. J. Math. Neurosci. **6**(1), 2 (2016)
6. M. Barahona, L.M. Pecora, Synchronization in small-world systems. Phys. Rev. Lett. **89**(5), 054101 (2002)
7. A. Barrat, M. Barthélemy, A. Vespignani, *Dynamical Processes on Complex Networks* (Cambridge University Press, Cambridge, 2008)
8. D.S. Bassett, E.T. Bullmore, Small-world brain networks revisited. Neuroscientist **23**(5), 499 (2016)

9. D.S. Bassett, O. Sporns, Network neuroscience. Nat. Neurosci. **20**(3), 353 (2017)
10. D.S. Bassett, P. Zurn, J.I. Gold, On the nature and use of models in network neuroscience. Nat. Rev. Neurosci. **19**(9), 566 (2018)
11. S. Boccaletti, V. Latora, Y. Moreno, M. Chavez, D.U. Hwang, Complex networks: structure and dynamics. Phys. Rep. **424**(4–5), 175 (2006)
12. S. Boccaletti, J. Almendral, S. Guan, I. Leyva, Z. Liu, I. Sendiña-Nadal, Z. Wang, Y. Zou, Explosive transitions in complex networks' structure and dynamics: percolation and synchronization. Phys. Rep. **660**, 1 (2016)
13. N.N. Bogoliubov, I.A. Mitropol'skii, Y.A. Mitropolsky, *Asymptotic Methods in the Theory of Non-Linear Oscillations*, vol. 10 (CRC Press, 1961)
14. R.M. Borisyuk, A.B. Kirillov, Bifurcation analysis of a neural network model. Biol. Cybern. **66**(4), 319 (1992)
15. M. Breakspear, Dynamic models of large-scale brain activity. Nat. Neurosci. **20**(3), 340 (2017)
16. E. Brown, J. Moehlis, P. Holmes, On the phase reduction and response dynamics of neural oscillator populations. Neural Comput. **16**(4), 673 (2004)
17. G. Buzsáki, *Rhythms of the Brain* (Oxford University Press, Oxford, 2006)
18. G. Buzsáki, A. Draguhn, Neuronal oscillations in cortical networks. Science **304**(5679), 1926 (2004)
19. O. Castejón, A. Guillamon, G. Huguet, Phase-amplitude response functions for transient-state stimuli. J. Math. Neurosci. **3**(1), 13 (2013)
20. P. Clusella, A. Politi, M. Rosenblum, A minimal model of self-consistent partial synchrony. New J. Phys. **18**(9), 093037 (2016)
21. A. Daffertshofer, R. Ton, B. Pietras, M.L. Kringelbach, G. Deco, Scale-freeness or partial synchronization in neural mass phase oscillator networks: pick one of two? NeuroImage (2018)
22. A. Daffertshofer, B. Pietras, Phase synchronization in neural systems, in *Encyclopedia of Complexity and Systems Science*, ed. by R.A. Meyers (Springer, Berlin Heidelberg, 2020), pp. 1–14
23. A. Daffertshofer, B. van Wijk, On the influence of amplitude on the connectivity between phases. Front. Neuroinformatics **5**, 6 (2011)
24. G. Deco, V.K. Jirsa, A.R. McIntosh, Emerging concepts for the dynamical organization of resting-state activity in the brain. Nat. Rev. Neurosci. **12**(1), 43 (2011)
25. R. Delabays, P. Jacquod, F. Dörfler, The Kuramoto model on oriented and signed graphs. SIAM J. Appl. Dyn. Syst. **18**(1), 458 (2019)
26. A. Dhooge, W. Govaerts, Y.A. Kuznetsov, H.G. Meijer, B. Sautois, New features of the software MatCont for bifurcation analysis of dynamical systems. Math. Comput. Model. Dyn. Syst. **14**(2), 147 (2008)
27. S.N. Dorogovtsev, A.V. Goltsev, J.F. Mendes, Critical phenomena in complex networks. Rev. Mod. Phys. **80**(4), 1275 (2008)
28. B. Ermentrout, *Simulating, Analyzing, and Animating Dynamical Systems: A Guide to XPPAUT for Researchers and Students* (SIAM, 2002)
29. G.B. Ermentrout, N. Kopell, Frequency plateaus in a chain of weakly coupled oscillators, I. SIAM J. Math. Anal. **15**(2), 215 (1984)
30. G. Ermentrout, N. Kopell, Oscillator death in systems of coupled neural oscillators. SIAM J. Appl. Math. **50**(1), 125 (1990)
31. G.B. Ermentrout, N. Kopell, Multiple pulse interactions and averaging in systems of coupled neural oscillators. J. Math. Biol. **29**(3), 195 (1991)
32. G.B. Ermentrout, D.H. Terman, *Mathematical Foundations of Neuroscience*, vol. 35 (Springer, New York, 2010)
33. H. Finger, R. Gast, C. Gerloff, A.K. Engel, P. König, Probing neural networks for dynamic switches of communication pathways. PLoS Comput. Biol. **15**(12), 1 (2019)
34. L.V. Gambuzza, A. Cardillo, A. Fiasconaro, L. Fortuna, J. Gómez-Gardeñes, M. Frasca, Analysis of remote synchronization in complex networks. Chaos **23**(4), 043103 (2013)
35. S. Gherardini, S. Gupta, S. Ruffo, Spontaneous synchronisation and nonequilibrium statistical mechanics of coupled phase oscillators. Contemp. Phys. **59**(3), 229 (2018)

36. A. Ghosh, Y. Rho, A.R. McIntosh, R. Kötter, V.K. Jirsa, Noise during rest enables the exploration of the brain's dynamic repertoire. PLoS Comput. Biol. **4**(10), e1000196 (2008)
37. C.M. Gray, Synchronous oscillations in neuronal systems: mechanisms and functions. J. Comput. Neurosci. **1**(1–2), 11 (1994)
38. S. Grossberg, Nonlinear neural networks: principles, mechanisms, and architectures. Neural Netw. **1**(1), 17 (1988)
39. P. Hagmann, L. Cammoun, X. Gigandet, R. Meuli, C.J. Honey, V.J. Wedeen, O. Sporns, Mapping the structural core of human cerebral cortex. PLoS Biol. **6**(7), e159 (2008)
40. H. Haken, *Advanced Synergetics: Instability Hierarchies of Self-organizing Systems and Devices*. Springer Series in Synergetics (Springer, Berlin, 1983)
41. H. Haken, *Synergetics: Introduction and Advanced Topics* (Springer Science & Business Media, 2013)
42. H. Haken, *Synergetics: Introduction and Advanced Topics* (Springer, Berlin, 2004)
43. J. Hlinka, S. Coombes, Using computational models to relate structural and functional brain connectivity. Eur. J. Neurosci. **36**(2), 2137 (2012)
44. C.J. Honey, R. Kötter, M. Breakspear, O. Sporns, Network structure of cerebral cortex shapes functional connectivity on multiple time scales. Proc. Natl. Acad. Sci. **104**(24), 10240 (2007)
45. F.C. Hoppensteadt, E.M. Izhikevich, *Weakly Connected Neural Networks* (Springer, New York, 1997)
46. E.M. Izhikevich, *Dynamical Systems in Neuroscience* (MIT press, 2007)
47. V.K. Jirsa, Neural field dynamics with local and global connectivity and time delay. Philos. Trans. R. Soc. Lond. A: Math., Phys. Eng. Sci. **367**(1891), 1131 (2009)
48. A.N. Khambhati, A.E. Sizemore, R.F. Betzel, D.S. Bassett, Modeling and interpreting mesoscale network dynamics. NeuroImage **180**, 337 (2018)
49. H. Kori, Y. Kuramoto, S. Jain, I.Z. Kiss, J.L. Hudson, Clustering in globally coupled oscillators near a Hopf bifurcation: theory and experiments. Phys. Rev. E **89**(6), 062906 (2014)
50. A. Koseska, E. Volkov, J. Kurths, Oscillation quenching mechanisms: amplitude versus oscillation death. Phys. Rep. **531**(4), 173 (2013)
51. Y. Kuramoto, *Chemical Oscillations, Turbulence and Waves* (Springer, Berlin, 1984)
52. W. Kurebayashi, S. Shirasaka, H. Nakao, Phase reduction method for strongly perturbed limit cycle oscillators. Phys. Rev. Lett. **111**(21), 214101 (2013)
53. Y.A. Kuznetsov, *Elements of applied bifurcation theory* (Springer, New York, 1998)
54. C.W. Lynn, D.S. Bassett, The physics of brain network structure, function and control. Nat. Rev. Phys. **1**(5), 318 (2019)
55. W.A. MacKay, Synchronized neuronal oscillations and their role in motor processes. Trends Cogn. Sci. **1**(5), 176 (1997)
56. I. Malkin, *Methods of Poincaré and Liapunov in Theory of Non-Linear Oscillations* (Gostexizdat, Moscow, 1949)
57. B. Monga, D. Wilson, T. Matchen, J. Moehlis, Phase reduction and phase-based optimal control for biological systems: a tutorial. Biol. Cybern. (2018)
58. J.Y. Moon, J. Kim, T.W. Ko, M. Kim, Y. Iturria-Medina, J.H. Choi, J. Lee, G.A. Mashour, U. Lee, Structure shapes dynamics and directionality in diverse brain networks: mathematical principles and empirical confirmation in three species. Sci. Rep. **7**, 46606 EP (2017)
59. J. Murdock, *Normal Forms and Unfoldings for Local Dynamical Systems* (Springer Science & Business Media, 2006)
60. H. Nakao, Phase reduction approach to synchronisation of nonlinear oscillators. Contemp. Phys. **57**(2), 188 (2016)
61. M. Newman, *Networks* (Oxford University Press, Oxford, 2018)
62. M. Newman, A.L. Barabási, D.J. Watts, *The Structure and Dynamics of Networks*, vol. 19 (Princeton University Press, Princeton, 2011)
63. V. Nicosia, M. Valencia, M. Chavez, A. Díaz-Guilera, V. Latora, Remote synchronization reveals network symmetries and functional modules. Phys. Rev. Lett. **110**(17), 174102 (2013)
64. J.M. Palva, S. Palva, K. Kaila, Phase synchrony among neuronal oscillations in the human cortex. J. Neurosci. **25**(15), 3962 (2005)

65. S. Petkoski, V.K. Jirsa, Transmission time delays organize the brain network synchronization. Philos. Trans. R. Soc. A **377**(2153), 20180132 (2019)
66. S. Petkoski, J.M. Palva, V.K. Jirsa, Phase-lags in large scale brain synchronization: methodological considerations and in-silico analysis. PLoS Comput. Biol. **14**(7), e1006160 (2018)
67. B. Pietras, A. Daffertshofer, Network dynamics of coupled oscillators and phase reduction techniques. Phys. Rep. **819**, 1 (2019)
68. M.A. Porter, J.P. Gleeson, Dynamical systems on networks. Front. Appl. Dyn. Syst.: Rev. Tutor. **4**, (2016)
69. J.G. Restrepo, E. Ott, B.R. Hunt, Synchronization in large directed networks of coupled phase oscillators. Chaos **16**(1), 015107 (2006). https://doi.org/10.1063/1.2148388
70. F.A. Rodrigues, T.K.D. Peron, P. Ji, J. Kurths, The Kuramoto model in complex networks. Phys. Rep. **610**, 1 (2016)
71. A. Rothkegel, K. Lehnertz, Recurrent events of synchrony in complex networks of pulse-coupled oscillators. Europhys. Lett. **95**(3), 38001 (2011)
72. A. Rothkegel, K. Lehnertz, Irregular macroscopic dynamics due to chimera states in small-world networks of pulse-coupled oscillators. New J. Phys. **16**(5), 055006 (2014)
73. P. Sanz-Leon, S.A. Knock, A. Spiegler, V.K. Jirsa, Mathematical framework for large-scale brain network modeling in the virtual brain. NeuroImage **111**, 385 (2015)
74. P. Sauseng, W. Klimesch, What does phase information of oscillatory brain activity tell us about cognitive processes? Neurosci. Biobehav. Rev. **32**(5), 1001 (2008)
75. B. Schack, S. Weiss, Quantification of phase synchronization phenomena and their importance for verbal memory processes. Biol. Cybern. **92**(4), 275 (2005)
76. H. Schuster, P. Wagner, A model for neuronal oscillations in the visual cortex. Biol. Cybern. **64**(1), 77 (1990)
77. M.A. Schwemmer, T.J. Lewis, The Theory of Weakly Coupled Oscillators, in *Phase Response Curves in Neuroscience: Theory, Experiment, and Analysis*, ed. by N.W. Schultheiss, A.A. Prinz, R.J. Butera (Springer Science & Business Media, New York, NY, 2012), pp. 3–31
78. S. Shirasaka, W. Kurebayashi, H. Nakao, Phase-amplitude reduction of transient dynamics far from attractors for limit-cycling systems. Chaos **27**(2), 023119 (2017)
79. S. Smale, *A Mathematical Model of Two Cells Via Turing's Equation, in The Hopf Bifurcation and Its Applications* (Springer, New York, 1976), pp. 354–367
80. M. Steriade, Cellular substrates of brain rhythms, in *Electroencephalography Basic Principles, Clinical Applications, and Related Fields*, ed. by E. Niedermeyer, F. Lopes Da Silva (Lippincott Williams & Wilkins, Philadelphia, 2005), pp. 31–84
81. S.H. Strogatz, Exploring complex networks. Nature **410**(6825), 268 (2001)
82. G. Thut, C. Miniussi, J. Gross, The functional importance of rhythmic activity in the brain. Curr. Biol. **22**(16), R658 (2012)
83. R. Ton, G. Deco, A. Daffertshofer, Structure-function discrepancy: inhomogeneity and delays in synchronized neural networks. PLoS Comput. Biol. **10**(7), e1003736 (2014)
84. F. Varela, J.P. Lachaux, E. Rodriguez, J. Martinerie, The brainweb: phase synchronization and large-scale integration. Nat. Rev. Neurosci. **2**(4), 229 (2001)
85. X.F. Wang, G. Chen, Synchronization in small-world dynamical networks. Int. J. Bifurc. Chaos **12**(01), 187 (2002)
86. D.J. Watts, S.H. Strogatz, Collective dynamics of 'small-world' networks. Nature **393**(6684), 440 (1998)
87. K.C. Wedgwood, K.K. Lin, R. Thul, S. Coombes, Phase-amplitude descriptions of neural oscillator models. J. Math. Neurosci. **3**(1), 2 (2013)
88. H.R. Wilson, J.D. Cowan, Excitatory and inhibitory interactions in localized populations of model neurons. Biophys. J. **12**(1), 1 (1972)
89. D. Wilson, B. Ermentrout, Greater accuracy and broadened applicability of phase reduction using isostable coordinates. J. Math. Biol. (2017)